Inorganic Chemistry

pubs.acs.org/IC

Article

Neutral Formazan Ligands Bound to the *fac*-$(CO)_3$Re(I) Fragment: Structural, Spectroscopic, and Computational Studies

Liliana Capulín Flores, Lucas A. Paul, Inke Siewert, Remco Havenith, Noé Zúñiga-Villarreal,* and Edwin Otten*

Cite This: *Inorg. Chem.* 2022, 61, 13532−13542

Read Online

ACCESS | Metrics & More | Article Recommendations | Supporting Information

ABSTRACT: Metal complexes with ligands that coordinate via the nitrogen atom of azo (N═N) or imino (C═N) groups are of interest due to their π-acceptor properties and redox-active nature, which leads to interesting (opto)electronic properties and reactivity. Here, we describe the synthesis and characterization of rhenium(I) tricarbonyl complexes with neutral *N*,*N*-bidentate formazans, which possess both N═N and C═N fragments within the ligand backbone (Ar^1-NH-N═C(R^3)-N═N-Ar^5). The compounds were synthesized by reacting equimolar amounts of [$ReBr(CO)_5$] and the corresponding neutral formazan. X-ray crystallographic and spectroscopic (IR, NMR) characterization confirmed the generation of formazan-type species with the structure *fac*-[$ReBr(CO)_3(\kappa^2$-N^2,N^4(Ar^1-N^1H-N^2═C(R^3)-N^3═N^4-Ar^5))]. The formazan ligand coordinates the metal center in the '*open*' form, generating a five-membered chelate ring with a pendant NH arm. The electronic absorption and emission properties of these complexes are governed by the presence of low-lying π*-orbitals on the ligand as shown by DFT calculations. The high orbital mixing between the metal and ligand results in photophysical properties that contrast to those observed in *fac*-[$ReBr(CO)_3$(L,L)] species with α-diimine ligands.

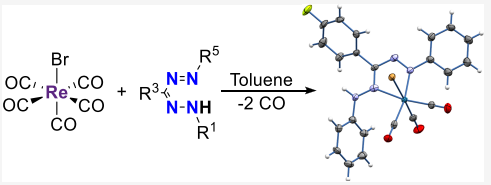

INTRODUCTION

Formazans are a large family of compounds containing the R^1-NH-N═C(R^3)-N═N-R^5 backbone, known for their use as analytical reagents for metal detection[1] and as cellular[2] and textile dyes.[3] These applications are the consequence of its well-defined redox chemistry[4] and its ability to chelate metal centers in its deprotonated form, i.e., the delocalized formazanate anion (R^1-N═N-C(R^3)═N-N-R^5)$^-$. Although formazanate coordination chemistry was first described in 1941,[5] it was not until the last decade that its study has reemerged due to its electrochemical and optical properties.[6] A wide variety of formazanate complexes with both main group and transition metal elements have been reported, wherein the (anionic) ligand usually coordinates through the terminal donor sites to form 6-membered chelates.[7] In addition to taking advantage of the unique optoelectronic properties imparted by formazanate ligands, recent reports show that their redox-active nature can also be used to obtain new catalytic reactivity.[8] In contrast to complexes with anionic formazanates, reports on coordination of the neutral formazan fragment remain scarce to date. In 2015, our group described the first example of a formazan-type complex,[9] in which the neutral ligand binds Zn(C_6F_5)$_2$ through one terminal and one internal nitrogen atoms yielding a five-membered chelate (Scheme 1), also described as the '*open*' coordination mode. It was hypothesized that the poor basicity of the Zn-C_6F_5 group in the precursor allowed the isolation of the Zn-formazan compound, as the more basic reagent $ZnMe_2$ does result in rapid deprotonation of the formazan NH group.[9]

Scheme 1. Synthesis of Zn Formazan Species

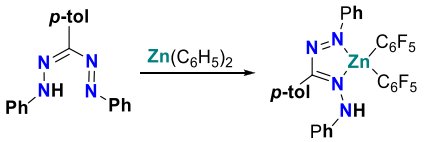

Formazan — 5-membered formazan *'open-form'*

Metal complexes with ligands containing the NH functionality have gained importance in catalysis since the NH arm can serve as an anchor for substrate recognition, thus enhancing catalyst selective and activity.[10] A proton source located at the proximity of the metal center has been widely investigated in the proton-coupled electron transfer reduction of small molecules relevant in energy conversion reactions such as hydrogen evolution[11,12] and CO_2 reduction.[13−15] It was proposed to modulate the redox properties, aid in the stabilization of intermediates, or impact the kinetics due to the increased local proton concentration. Furthermore, deprotonation of the NH group is known to modify the electronic and geometric structure of such complexes.[16−18]

Received: June 22, 2022
Published: August 15, 2022

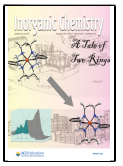

https://doi.org/10.1021/acs.inorgchem.2c02168
Inorg. Chem. 2022, 61, 13532−13542

Chart 1. Representative Examples of Re Complexes Bearing an XH Functionality

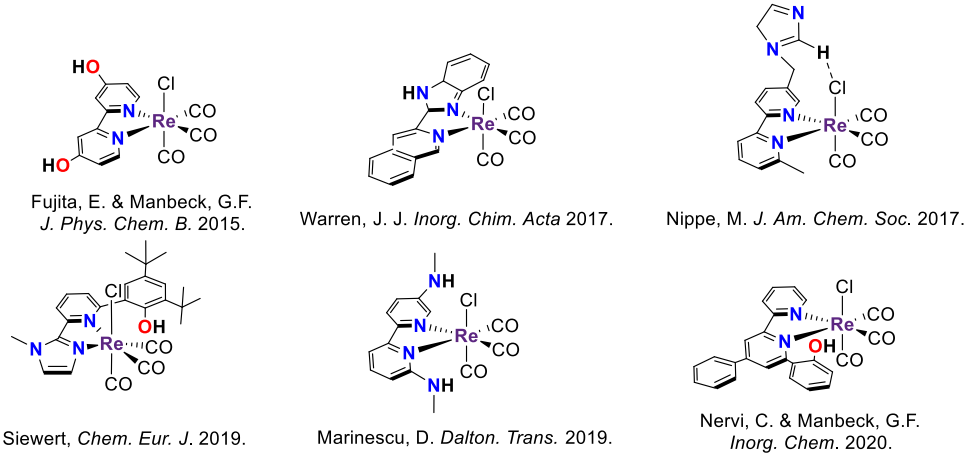

Scheme 2. Synthesis of Formazan Ligands

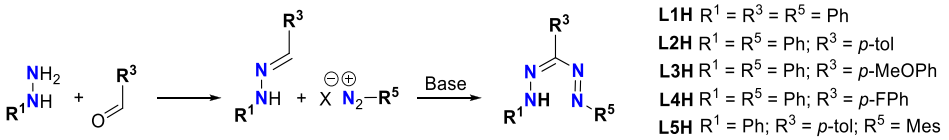

Scheme 3. General Synthesis of Compounds (a) 1−4 and (b) the Mixture of Isomers 5a and 5b

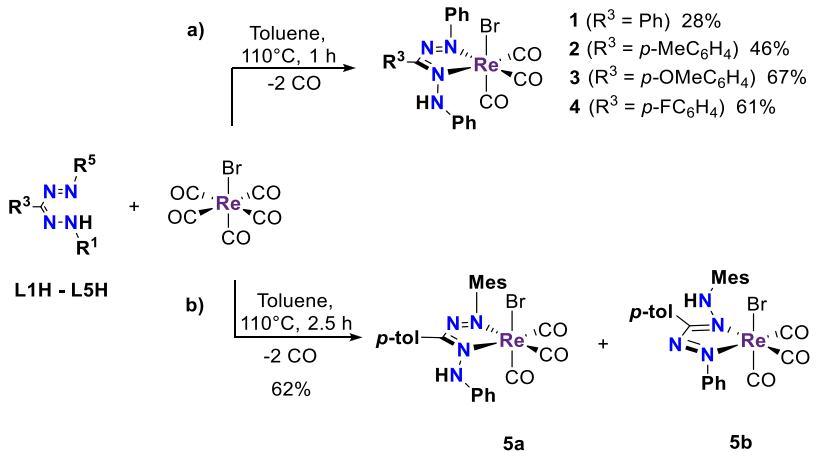

Extensive research has focused on the properties and potential applications of *fac*-[L,LReX(CO)$_3$] (L = α-diimine) compounds in medicinal inorganic chemistry,[19,20] material science,[21,22] and catalysis.[23,24] Particularly, these compounds have shown to be good candidates for electrochemical CO_2 reduction, in which a proton source is required either for enhancing or triggering the catalytic process.[25,26] Mainly, Re-based bipyridine systems have been reported as catalysts for CO_2 electroreduction, wherein the presence of XH (X = O, N, C)[18,27,28] functionalizations boosts the catalytic effect or induces other reactivity patterns (Chart 1).[29−31] Key to the catalytic conversion of CO_2 to CO by the well-studied bipyridine Re and Mn complexes is the involvement of the supporting ('redox-active') ligand in the reduction chemistry.[28,32−34] We hypothesize that replacing the bipyridine ligand (an aromatic α-diimine) for a redox-active formazan ligand (formally an amino-substituted α-azoimine) could provide an avenue to influence the potential at which reduction of the catalyst occurs.[35,36] In addition, such ligands provide access to flexible coordination modes (hemilability)[37] due to the presence of four nitrogen atoms in the backbone, as well as proton-responsivity via the NH moiety that is in close proximity to the metal center, features that are key to the activity/selectivity of metalloenzymes but challenging to emulate in synthetic catalysts.[38]

Herein, we report synthesis of a series of *fac*-Re(CO)$_3$(formazan) complexes and investigate their (electronic) structures and photophysical properties.

RESULTS AND DISCUSSION

Ligand Synthesis. Formazan ligands **L1H**−**L4H** were synthesized according to the procedure reported by Hicks and coworkers, via aldehyde condensation with phenylhydrazine followed by a coupling reaction with phenyldiazonium chloride in a biphasic reaction medium (CH_2Cl_2/water) under mild basic conditions.[4] Similarly, **L5H** was prepared using the methodology previously described by our group, in which the coupling step is carried out in acetone/water with NaOH as

https://doi.org/10.1021/acs.inorgchem.2c02168
Inorg. Chem. 2022, 61, 13532−13542

base (Scheme 2).[9] In all cases, the compounds were obtained in moderate yields after purification (27−54%).

Complex Synthesis. Equimolar amounts of $[ReBr(CO)_5]$ and the corresponding formazan, **L1H**−**L4H**, reacted in refluxing toluene for 1 h to afford complexes **1**−**4** in moderate to good yields (28−67%) (Scheme 3a). In all cases, complete conversion of the starting material was confirmed by ^{1}H NMR and infrared spectroscopy. The compounds are air-stable solids with dark red color and are soluble in low to medium polarity solvents. Complexes **2**−**4** were isolated as pure materials by either recrystallization or rinsing with pentane. A minor impurity was invariably present (^{1}H NMR spectroscopy) in the isolated material of **1**. Attempts to further purify the material by crystallization were unsuccessful. The reaction of the asymmetric formazan **L5H** with $[ReBr(CO)_5]$ in refluxing toluene gave a mixture of two complexes (**5a** and **5b**) based on ^{1}H NMR spectroscopy (Scheme 3b), which differ in the substituent at the NH position (Mes or Ph). Unsurprisingly, complexes **5a**/**b** present similar physical properties—dark red solids soluble in low polarity solvents—that we were unable to separate, and solution characterization data are reported below for the mixture.

FT-IR Spectroscopy. The infrared spectra of complexes **1**−**4** and the mixture **5a**/**b** feature the characteristic pattern for *fac*-tricarbonyl species: three intense bands in the ν(CO) carbonyl region arising from the IR-active 3A normal vibration modes for complexes with a C_1 symmetry (Figure 1). The CO

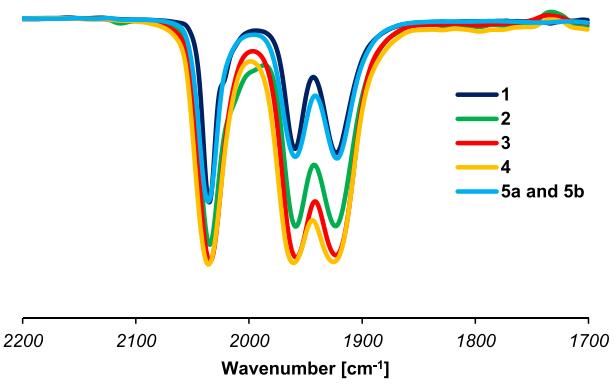

Figure 1. CO stretching bands (ν(CO)) in the FT-IR spectra of complexes **1**−**4** and the mixture **5a** and **5b** in CH_2Cl_2 solution at rt.

stretching frequencies for compound **1** are observed at 2035, 1959, and 1923 cm^{-1} in CH_2Cl_2 solution. The effect of the *para*-substituent on the aromatic ring (R^3) is minimal, and compounds **2**−**5** show virtually identical IR spectra.

NMR Studies. ^{1}H NMR spectra of **1**−**4** show a singlet ca. 8.5 ppm assigned to the hydrazo proton, consistent with the presence of a neutral formazan ligand (see Figure S1a−S4a). In agreement with the presence of an asymmetric, protonated formazan ligand, the ^{13}C NMR spectrum shows three distinct carbonyl resonances between 185 and 192 ppm indicative of C_1 symmetry for these Re complexes. In ^{13}C NMR spectroscopy, the N-Ph *ipso*-carbon atoms attached to the formazan backbone display distinctive chemical shifts. Unequivocal assignment of these was possible based on an HSQC experiment where coupling between the hydrazo NH group and one of the Ph *ipso*-C resonances was observed. The resonance of the *ipso*-C bound to the azo group appears at 157 ppm, which is downfield from both the *ipso*-C linked to the NH function located ca. 141 ppm, and the *ipso*-C of the C-Ar group (120−125 ppm). Similarly, the N-Ph groups are inequivalent in the ^{1}H NMR spectrum also at elevated temperature (80 °C in toluene-d_8), suggesting that chemical exchange by proton transfer between the azo (C-N═N-Ph) and hydrazo (C═N-NH-Ph) fragments does not readily occur. This was further corroborated by the absence of exchange crosspeaks in the 2D EXSY spectrum (80 °C, mixing time of 0.5 s, Figure S7).

^{1}H NMR analysis of the reaction mixture of complexes **5a**/**b** indicates the generation of two main products in ratio of 0.7:1.0 with both compounds exhibiting the characteristic NH proton signal of the neutral formazan ligand at 8.15 and 7.60 ppm, respectively (Figure 2a). Minor signals for another species were observed (<5%) but not investigated further. For the two major products, the observation of eight unique resonances in the aliphatic region of the ^{1}H and ^{13}C NMR spectra indicates that all CH_3 groups are inequivalent: each of the two products features four signals due to the CH_3 substituents at the *p*-tolyl (1) and mesityl (3) rings. Thus, at room temperature, the rotation around the N-Mes bond is slow on the NMR timescale. In the most downfield part of the ^{13}C{^{1}H} NMR spectrum, i.e., between 180 and 200 ppm, there are six resonances that can be attributed to carbonyl ligands, which corroborates that both **5a** and **5b** are tricarbonyl rhenium complexes (Figure S6). Based on the spectroscopic data, we assign **5a** and **5b** as two different isomers with the composition $[(\mathbf{L5H})Re(CO)_3Br]$, which differ in the nature of the 'pendant' (non-coordinating) N-Ar group of the formazan (see Scheme 3b). Heating an NMR tube containing the mixture of complexes **5a**/**b** to 80 °C inside the NMR spectrometer did not significantly change their molar ratio. Inspection of 2D NMR experiments allowed the assignment of ^{1}H and ^{13}C spectra (see Figure S6). Identification of the *m*-CH (Mes) and the *m*- and *o*-CH (*p*-tolyl) protons allowed establishing of the connectivity in both of the isomeric compounds present in solution. The ^{1}H,^{13}C correlations in the HMBC spectrum between the NH fragment and the carbon atoms that are two and three bonds away indicate that in the major isomer (**5b**), the NH group is bound to a mesityl group, whereas in **5a** it is connected to a phenyl group. The greater shielding effect of mesityl compared to the phenyl group causes the NH proton of the former to appear at higher field (δ 7.61 ppm in **5b** and 8.22 ppm in **5a**).

To investigate the dynamics of isomers **5a**/**b** in solution, we collected a ^{1}H EXSY NMR spectrum at 80 °C in toluene-d_8 (Figure 2b). Crosspeaks are observed between the Mes *ortho*-CH_3 groups within each isomer due to rotation around the N-Mes bond but not between isomers **5a** and **5b**. Whereas free formazans undergo intramolecular proton exchange rapidly ('tautomerization'),[39,40] the lack of exchange between **5a**/**b** indicates that the Re−N bonds are non-labile and coordination to the Re center effectively blocks exchange. This is in agreement with the data for the symmetrical derivative **4**, which also does not show exchange between the azo and hydrazo fragments (*vide supra*). It should be noted however that the EXSY spectrum does evidence exchange between the NH groups in **5a**/**b**, which we believe to occur by an intermolecular pathway instead. This is further corroborated by the observation of exchange crosspeaks between the NH protons in **5a**/**b** and residual H_2O when the NMR solvent is not fully anhydrous (Figure S8).

https://doi.org/10.1021/acs.inorgchem.2c02168
Inorg. Chem. 2022, 61, 13532−13542

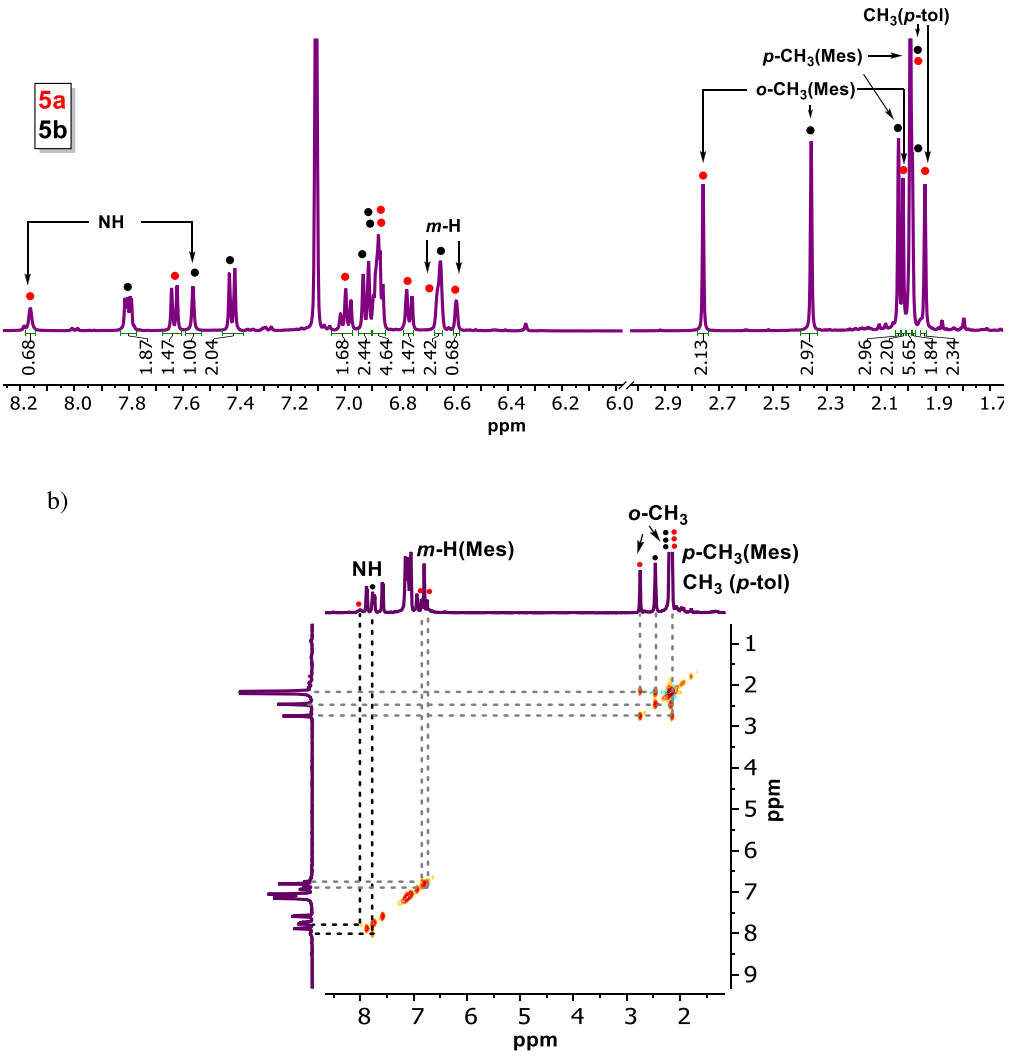

Figure 2. (a) ^{1}H NMR spectrum of the mixture **5a** and **5b** at room temperature in benzene-d_6. (b) EXSY experiment at 80 °C in toluene-d_8.

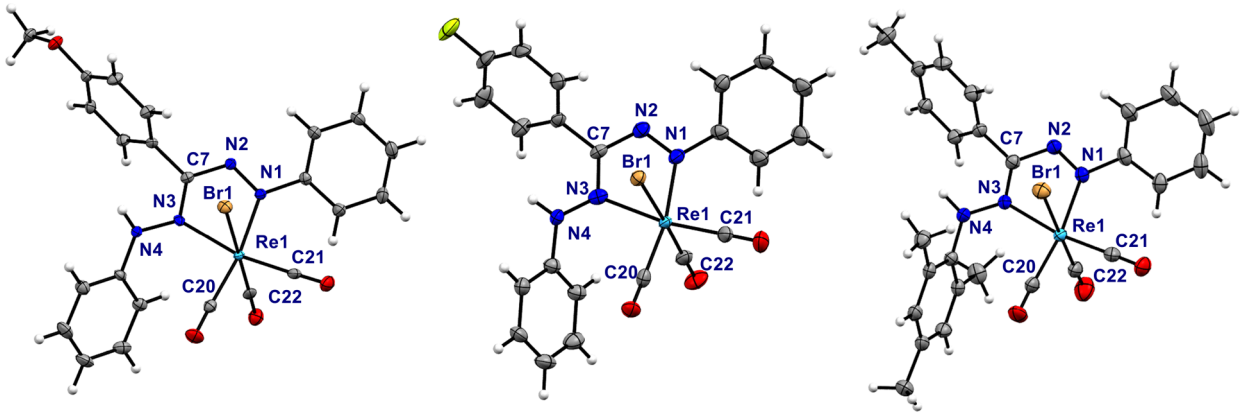

Figure 3. Molecular structures of **3** (left), **4** (middle), and **5b** (right) showing 50% of ellipsoids.

Additional experiments were conducted to determine whether intermolecular proton interchange processes also place in the complexes containing a symmetric formazan ligand. Partial H/D exchange of the NH proton in complex **4** was achieved by mixing a $CDCl_3$ solution of the aforementioned complex with D_2O. ^{1}H NMR analysis of the resulting mixture indicated that it was composed of 60% **4D** (deuterated product) and 40% the non-deuterated species **4**. The remaining D_2O was subsequently removed by stirring over $MgSO_4$, the **4**/**4D** mixture was isolated and then reacted with an equivalent of **2** in C_6D_6. Monitoring the composition by ^{1}H NMR spectroscopy showed that the intensity of the NH resonance of **4** increased (to 72%) in the course of 30 min with a concomitant decrease of that in **2**, confirming that intermolecular proton exchange is taking place (see Figure S9).

https://doi.org/10.1021/acs.inorgchem.2c02168
Inorg. Chem. 2022, 61, 13532−13542

Structural Studies. Crystals suitable for single-crystal X-ray diffraction were obtained from slow diffusion of pentane into a $CHCl_3$ solution of compounds **3** and **4**, respectively. The mixture of **5a/b** did not crystallize using the same method, but we were able to obtain a microcrystalline sample from hot hexane that contained some small needles that were suitable for X-ray crystallographic characterization. This was identified as isomer **5b**, in which the sterically most demanding Mes group is situated at the non-coordinated N atom of the ligand; the solid-state structure observed for this material is consistent with the major species in solution by NMR spectroscopy. Analysis of the molecular structures of **3**, **4**, and **5b** shows that the three compounds are isostructural (see Figure 3 and Table 1 for pertinent bond lengths and angles). The geometry around the metal center is pseudo-octahedral with the carbonyl ligands in a facial arrangement. The formazan fragment coordinates in a bidentate fashion through atoms N1 and N3, generating a five-membered chelate. Coordination of the neutral formazan is scarce, only observed in the complex [**L2H**]$Zn(C_6F_5)_2$ previously reported by our group.[9] The formazan bite angles are virtually identical in the three complexes (**3** = 73.04(9)°, **4** = 73.0(2)°, **5b** = 72.9(1)°) and somewhat smaller than the bite angle reported for the [**L2H**]$Zn(C_6F_5)_2$ complex (74.23(13)°). The C7−N2 and C7−N3 bond lengths are different from each other, the magnitude of the C7−N3 bond lies in between the typical values for C−N single and double bonds (−C(sp^2)−N− = 1.355 Å; −C(sp^2)=N− = 1.279 Å), while the C7−N2 bond length indicates a single bond character. The N1−N2 bond length is longer than a N=N double bond (−N=N− = 1.240 Å) and smaller than a N−N single bond (−N−N− = 1.425 Å).[41] The metallacycle is not fully planar as the Re atom is displaced out of the ligand plane (N1−N2−C7−N3) by 0.213−0.393 Å. The dihedral angle between the ligand plane and a phenyl group in the R^1 position is similar in complexes **3** (50.67°) and **4** (51.12°). Changing the R^1 substituent for the bulkier mesityl group (**5b**) causes a rotation out of the ligand plane by almost 30° resulting in a dihedral angle of 79.52° that prevents steric interactions between the Mes substituent and the equatorial CO ligand. The structure indicates that rotation around the N-Mes bond cannot occur freely due to these steric interactions, which is in agreement with the solution NMR data discussed above. The Re1−N1 bond length to the azo moiety is virtually the same in the three complexes (2.099−2.126 Å) but it is shorter than the Re−N(azo) bond length reported for the related [$ReBr(CO)_3$(azopyridine)][42] complex (2.156(3) Å). The Re1−N3 bond lengths are in accordance with the typical Re−N(imine) bond distances (2.173−2.185 Å in compounds **3**−**5** *vs* 2.173(3) Å in [$ReBr(CO)_3$(6-methoxipyridine-2-yl)-*N*-(2-methylthiophenyl)methanimine)], respectively).[43] The unusually short Re−N1(azo) bond length reflects that π-backdonation from the Re center to the azo group is more pronounced in the formazan species than in azopyridine complexes.[44] The π-acceptor capabilities of the azo ligand are also reflected in the Re−carbonyl bond lengths. The Re−C20 bond length, *trans* to the azo group, is longer than the Re−C21 bond length. This is consistent with the considerable π-acidity of the azo group,[45,46] which appears to be more significant in our formazan complexes than in the corresponding azopyridine analogues.[42]

Table 1. Selected Metrical Parameters for 3, 4, and 5b (Bond Lengths in Å, Angles in °)

	3	4	5b
Re1−Br1	2.5977(3)	2.6236(7)	2.5946(6)
Re1−N1	2.126(2)	2.099(6)	2.122(3)
Re1−N3	2.173(3)	2.185(5)	2.174(4)
Re1−C20	1.955(3)	1.955(6)	1.957(5)
Re1−C21	1.921(3)	1.919(5)	1.916(6)
Re1−C22	1.941(2)	1.918(6)	1.964(4)
N1−N2	1.298(3)	1.291(7)	1.293(5)
C7−N2	1.363(4)	1.382(7)	1.364(8)
C7−N3	1.330(4)	1.319(8)	1.326(5)
N3−N4	1.343(4)	1.324(8)	1.343(7)
Br1−Re1−C22	178.02(9)	176.8(2)	178.6(2)
N1−Re1−C20	170.3(1)	168.7(2)	170.2(2)
N3−Re1−C21	166.5(1)	169.7(2)	170.3(2)
N1−Re1−N3	73.04(9)	73.0(2)	72.9(1)

UV−vis Spectroscopy. The electronic spectra of complexes **1**−**4** and the mixture of complexes **5a/5b** were measured at 25 °C in toluene ($c \approx 10^{-5}$ M), Figure 4. Their corresponding data are summarized in Table 2. Compounds **1**−**4** show similar features: an intense band in the range of 490−510 nm with maximum molar absorptivities from 18,000 to 28,000 M^{-1} cm^{-1}. DFT calculations and comparison to literature data allows us to assign this band to electronic excitations that are Re(d_π) → azo(π^*)[42] MLCT and formazan $\pi \rightarrow \pi^*$ in nature.[9] A band of lower intensity in the range of

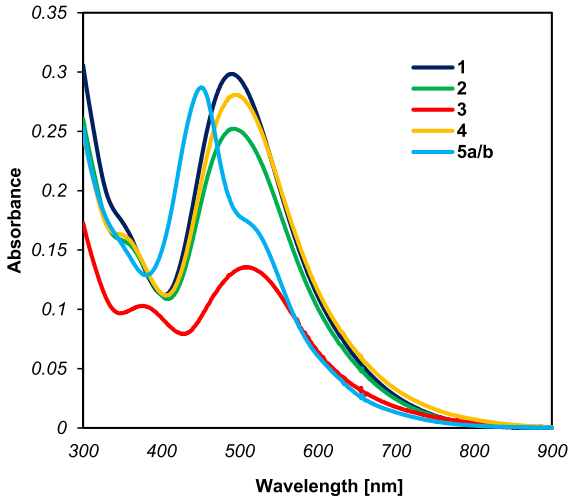

Figure 4. Absorption spectra for compounds **1**−**4** and **5a/b** in toluene solution.

Table 2. UV−vis Absorption Data

compound	λ_{max} (nm)	ε (M^{-1}·cm^{-1})	λ_{max} (nm)	ε (M^{-1}·cm^{-1})
1	356	16,500	490	18,100
2	353	15,300	485	19,400
3	375	10,500	509	14,100
4	353	15,300	495	27,000
5a/b			452	
			~520[a]	

[a]Approximate band position due to its appearance as a shoulder on the more intense absorption of the other isomer.

https://doi.org/10.1021/acs.inorgchem.2c02168
Inorg. Chem. 2022, 61, 13532−13542

330−400 nm (ε =15,000−16,500 M^{-1} cm^{-1}) is observed in all compounds. While bands at similar energies are typically assigned to metal-to-ligand charge transfer in related compounds,[47,48] time-dependent DFT calculations for **4** instead indicate little involvement of the Re d-orbitals in this transition (*vide infra*). Overall, the λ_{max} values of **1**, **2**, and **4** do not differ significantly, suggesting that the substituent at the *para*-position of the N-Ar rings has little influence on the energy of the electronic transitions, which is in line with the notion that the acceptor orbital in these transitions is a formazan π^*-orbital that is relatively insensitive to the *para*-substituent. In the case of complex **3**, λ_{max} is slightly red-shifted (509 nm) compared to complex **1** (490 nm), indicating that the involvement of the π-donating OMe group on the conjugated system is noticeable. When the spectrum of **4** was recorded in acetonitrile, a modest hypsochromic shift was observed (λ_{max}^{AcCN} = 483 nm (Figure 6a); $\lambda_{max}^{Toluene}$ = 495 nm), showing that these species manifest a small, negative solvatochromism. Comparing λ_{max} values to those reported for complexes with anionic formazanate ligands,[9,49,50] the absorption maxima in **1**−**4** are blue-shifted due to a smaller extent of π-conjugation within the backbone of the neutral ligands compared to the fully delocalized anions. The mixture of complexes **5a**/**b** features two intense bands at 520 and 452 nm derived from the MLCT and $\pi-\pi^*$ formazan electronic transitions and a shoulder at 350 nm. Overall, the influence of the substituents on the lowest energy band is more pronounced when they are located at the N=N and NH formazan positions, similar to what was observed in complexes with anionic formazanate ligands.[6] Clearly, the nature of electronic absorptions for the two isomers **5a**/**b** is quite distinctive, as is manifested by the significant shift in λ_{max}.

Density Functional Theory (DFT) Calculations. For representative complexes **4** and **5a**/**b**, geometry optimizations were carried out in the ground state using density functional theory (DFT; MN15L[51] functional and def2-TZVP[52] basis set) using the crystallographic coordinates as a starting point. The geometries were confirmed to be minima on the potential energy surface by frequency calculations (no imaginary frequencies); the resulting structures are in good agreement with the metrical parameters obtained from X-ray diffraction (complexes **4** and **5b**), albeit that the Re−Br and hydrazo N−N bonds are slightly overestimated (Tables S2 and S3). Analysis of the frontier orbitals at the optimized geometry of **4** showed that the HOMO is mainly localized on the [ReBr(CO)$_3$] core and is composed of a Re d_π orbital that is antibonding with a bromine *p* orbital and π-bonding with the CO ligand located *trans* to Br. The HOMO level also contains some ligand character (the hydrazo-phenyl fragment). On the other hand, the LUMO is primarily a π^*-orbital of the formazan framework, with a minor Re 5*d* character (Figure S10).

The optimized structures of **5a** and **5b** are overall similar, but the variation in the position of the Mes group (on the *azo* or *hydrazo* N-atom, respectively) leads to somewhat different frontier orbitals. While those of **5b** are similar to **4**, the HOMO of **5a** has noticeably smaller formazan contribution (Figures S12 and S14). The relative stability between the isomeric forms **5a** and **5b** was also evaluated based on these DFT calculations. Using the gas phase geometries, the Gibbs free energy difference between both compounds was computed in toluene solution using the solvation energies from SMD calculations and found to be 1.6 kcal/mol at room temperature, with **5b** being the most stable isomer. Qualitatively, the trend in relative stability is consistent with our empirical data since compound **5b** is the predominant species in the reaction mixture according to the NMR integration. It should be noted that it is also possible that the **5a**/**5b** ratio found experimentally is kinetically controlled as no interconversion between both isomers was observed.

Time-dependent density functional theory (TDDFT) calculations were carried out on complex **4** as a representative example. Relevant excitations were analyzed in more detail using natural transition orbital calculations (NTOs) to provide insight into their nature. According to the calculations, the three lowest-energy transitions in **4** (λ_{calc} = 645, 539 and 526 nm) all have small oscillator strength and involve transitions from orbitals centered on the [ReBr(CO)$_3$] fragment (π^*(Re-Br) and (π(Re-CO)) into the formazan π^*-orbital. The fourth excited state, with the highest oscillator strength in the visible range (λ_{calc} = 487 nm; $\lambda_{max,exp}$ = 495 nm, Figure S11a-b), has a more pronounced formazan (intraligand) $\pi-\pi^*$ character, involving an occupied azo π-orbital as the donor (see Table S4 for the corresponding NTO), but also here the contribution of metal-based orbitals is still clearly noticeable. Thus, in all excitations in the visible range, there is extensive mixing between the metal and ligand orbitals in the ground and excited states, which results in electronic transitions of mixed nature: all show contributions from MLCT Re(dπ) → formazan(π^*), LLCT Br(*p*) → formazan(π^*), and ILCT azo(π) → formazan(π^*) excitations. The strong metal−ligand orbital mixing results in reduced charge transfer character in the MLCT bands, which is reflected in the minor influence of solvent polarity (toluene *vs* acetonitrile) on the empirical electronic absorption spectrum (*vide supra*).[53] Similar to the absorptions in the visible range, analysis of the NTOs of the higher energy transitions shows that these involve the formazan π^*-orbital as the acceptor and are also highly mixed in character.

TDDFT calculations were performed on the optimized structures of complexes **5a**/**b** to understand the impact of the pendant R^1/R^5 arms on the electronic transitions. The intense low-energy absorption is computed to be shifted to higher energy for **5a** (444 nm) compared to **5b** (489 nm), see Figures S13 and S14, respectively. This is in agreement with the empirical UV/vis spectrum, which shows two distinct bands at 452 and 520 nm for the **5a**/**b** mixture. As in **4**, the natural transition orbital pair for the main low-energy excitation in **5b** consists of a 'hole' NTO on the [ReBr(CO)$_3$] core, whereas the excited electron ('particle' NTO) consists primarily of the π^* formazan orbital. A comparison of the NTOs for **5a** and **5b** shows that the main difference between the two isomers is found in the hole NTO (Figure 5), which has a higher formazan contribution in **5a**. Based on the optimized geometries, the orientation of the azo-NAr ring changes upon swapping the aryl groups on the nitrogen atoms (Ph/Mes): the angle between the plane defined by the five-membered chelate ring and the Mes-substituent is 73.77° in **5a**, whereas the corresponding angle with the Ph-substituent in **5b** is only 39.28°. To test our hypothesis that the orientation of the azo-NAr group has a major impact on the spectral properties, we took the geometry of **5b** and rotated the N-Ph group out of the ligand plane to be in the same orientation as the N-Mes group in **5a**. This structure is labeled **5b_rot**. The main visible band in the TDDFT spectrum calculated at the **5b_rot** geometry is blue-shifted by 30 nm (1342 cm^{-1})

https://doi.org/10.1021/acs.inorgchem.2c02168
Inorg. Chem. 2022, 61, 13532−13542

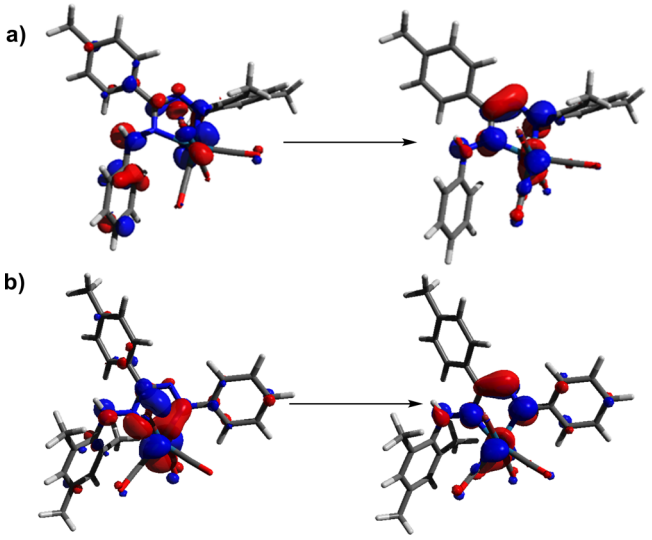

Figure 5. Natural transition orbitals for the highest-intensity excitation in the visible (isovalue = 0.05) for (a) **5a** and (b) **5b** represented as a hole → electron.

compared to **5b**, but the other transitions remain at similar energies (Figure S17). An analysis of the orbital mixing between the azo-NAr ring and the rest of the ligand π-system confirms that rotating the Ar ring out of the plane disrupts conjugation (Table S7), and thus we conclude that this is responsible for the spectral shift observed.

Luminescence Spectroscopy. The emission spectrum of **4** measured at room temperature in acetonitrile using an excitation wavelength of 320 nm shows a broad featureless emission band at 380 nm (Figure 6a). The excited state showed a monoexponential decay (λ_{ex} = 370 nm) with a lifetime (τ) of 3.69 ns under a N_2 atmosphere, which does not appreciably change under O_2 (τ = 3.60 ns) (see Figure S19). Furthermore, the excitation spectrum (λ_{em} = 380 nm) exhibits a broad band centered at 310 nm (Figure 6b). In contrast to the majority of *fac*-[ReX(CO)$_3$(L,L)] complexes with bidentate N-donor ligands (e.g., α-diimines), which typically show emission at higher wavelengths (400−600 nm),[54,55] this data shows that the triplet (metal−ligand or ligand-centered)[56] excited states typical for the photoluminescence of *fac*-[ReX(CO)$_3$(L,L)] compounds[57] are non-emissive in formazan Re(I) species. This also stands in contrast to complexes with anionic formazanate ligands, which show highly tunable emission with large Stokes shifts at much lower energies.[58−60]

CONCLUSIONS

We described the straightforward synthesis of the first complexes bearing the neutral formazan ligand toward a group 7 metal. The *fac*-(CO)$_3$ReBr(formazan) complexes obtained contain a five-membered chelate ring, in which the ligand binds via the nitrogen atoms of the azo (N=*N*-Ar) and hydrazo (C=*N*-NHAr) groups, which leaves a pendant acidic (exchangeable) NH moiety in close proximity to the metal center. Structural and spectroscopic data demonstrate that the formazan ligand is tightly bound to the metal center, which is due to the strong π-acceptor character of the ligand. The effect of ligand substituents on the properties of the complexes is only minor, but the preparation of an asymmetric derivative with a N-Mes substituent demonstrates that changes in the sterics shift the electronic absorption spectrum due to changes

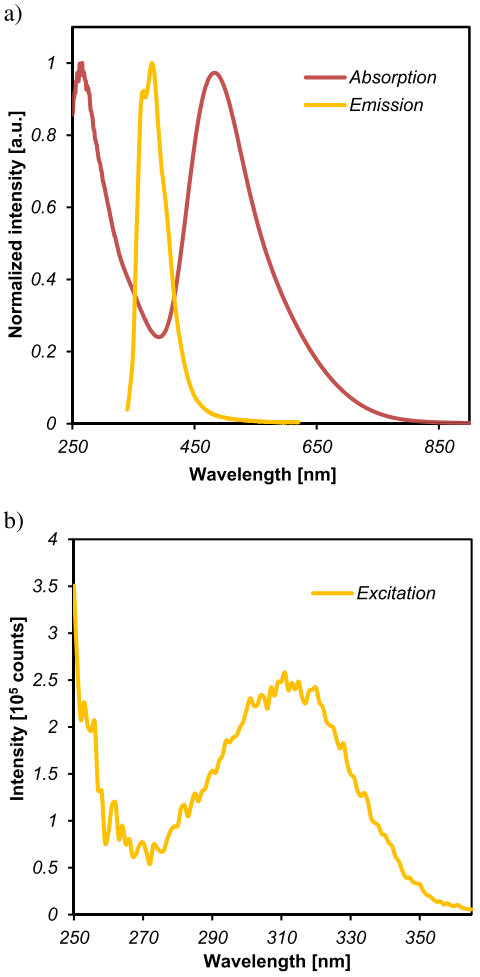

Figure 6. (a) Normalized absorption and emission spectra of **4** in MeCN recorded at λ_{exc} = 320 nm; (b) excitation spectrum of **4** in MeCN. The data were collected at room temperature.

in the conjugation within the ligand. Computational studies at the DFT level confirm a high degree of covalency in the metal-formazan interaction and highly mixed metal−ligand character of the frontier orbitals, which is sensitive to the degree of conjugation within the ligand as demonstrated by sterically switching 'off' π-interactions in the derivative with a N-Mes group (compound **5a**). Unlike many *fac*-[ReX(CO)$_3$(L,L)] compounds (L,L = α-diimine ligands) reported in the literature, our formazan complexes are only weakly luminescent in the near-UV (λ_{em} = 380 nm), and emission from the lower-energy excited states is not observed. In ongoing work, we are investigating the possibility of using the proton-responsive nature of the NH group (i.e., formazan/formazanate interconversion) in 'cooperative' reactivity of this type of complexes.

EXPERIMENTAL SECTION

General Considerations. All work—except ligand synthesis—was conducted under a nitrogen atmosphere using conventional Schlenk and vacuum-line techniques. Pentane and toluene (Aldrich, anhydrous. 99.8%) were passed over columns of Al_2O_3 (Fluka) and BASF R3-11-supported Cu oxygen scavengers. [ReBr(CO)$_5$] was prepared according to the published procedures[61] from [Re$_2$(CO)$_{10}$] (Aldrich, 98%) and Br_2 (Aldrich, 98%). The ligands 1,5-diphenyl-3-*p*-tolylformazan (**L2H**), 1,5-diphenyl-3-*p*-methoxyphenylformazan (**L3H**), and 1,5-diphenyl-3-*p*-flourophenylformazan (**L4H**) were

https://doi.org/10.1021/acs.inorgchem.2c02168
Inorg. Chem. 2022, 61, 13532−13542

Table 3. Crystallographic Data for 3, 4, and 5b

	3	4	5b
chemical formula	$C_{23}H_{18}BrN_4O_4Re$	$C_{22}H_{15}BrFN_4O_3Re$	$C_{26}H_{24}BrN_4O_3Re$
M_r	680.52	668.49	706.6
cryst syst	triclinic	monoclinic	triclinic
color, habit	purple, needle	purple, needle	purple, block
size (nm)	0.42 ×0.13× 0.04	0.70 × 0.170 × 0.060	0.40 × 0.33 × 0.20
space group	$P\bar{1}$ (No.2)	$P21/n$ (No.14)	$P\bar{1}$ (No.2)
a (Å)	9.0463(6)	10.095(2)	9.9235(12)
b (Å)	11.0459(7)	18.586(6)	10.9196(13)
c (Å)	12.7033(8)	12.219(4)	13.0134(15)
α (deg)	107.379(2)	90	77.085(4)
β (deg)	94.935(3)	107.191(8)	72.218(4)
γ (deg)	103.227(2)	90	75.163(4)
V (Å^3)	1162.89(13)	2190.1(11)	1281.7(3)
Z	2	4	2
ρ_{calc} (g·cm^{-3})	2.302	2.027	1.831
radiation, λ (Å)	Mo, Kα, 0.71073	Mo, Kα, 0.71073	Cu, Kα, 1.54178
μ(Mo, Kα) (mm^{-1})	8.777	7.413	11.384
F(000)	750	1272	684
temp (K)	100(2)	100(2)	100(2)
θ range (deg)	3.028−27.191	3.044−27.200	3.612−70.304
data collected (h, k, l)	−11:11, −14:14, −16:16	−12:12, −23:23, −15:15	−12:12, −13:13, −15:15
no. of reflns collected	45,523	27,390	21,942
no. of indep reflns	5166	4818	4526
obsd reflns $F_o \geq 2.0\sigma(F_o)$	4966	4288	4396
$R(F)$ [obsd reflns] (%)	1.78	2.81	2.19
$R_w(F^2)$ [all reflns] (%)	5.24	6.13	5.51
GOF	1.051	1.192	1.119
weighting a, b	0.03300, 1.26140	0.0000, 12.4515	0.0000, 2.9889
params refined	303	293	324
min, max residual densities	−1.04, 1.32	−1.61, 1.82	−0.83, 0.85

synthesized using the methodology reported by Hicks and coworkers.[4] Particularly, 5-mesityl-1-phenyl-3-*p*-tolylformazan (**L5H**) was prepared using a modified procedure published by our group.[9] 1,3,5-Triphenylformazan (**L1H**, TCI, 92%), *p*-tolualdehyde (Aldrich 97%), 4-methoxybenzaldehyde (Aldrich, 98%), 4-fluorobenzaldehyde (Aldrich, 98%), phenylhydrazine (Aldrich, 99%), aniline (Aldrich 99%), sodium nitrite (Aldrich, 99%), sodium carbonate (Aldrich, 99.5%), and [NBu_4]Br were used as received. $CHCl_3$ (Aldrich, 99%) and $CDCl_3$ (Aldrich, 99.8 atom %D) were used without further purification.

NMR spectra were measured on Mercury 400, Varian Inova 500, or Bruker 600 MHz spectrometers. Residual solvent signals were used as internal reference for ^{1}H and ^{13}C spectra and reported in ppm relative to TMS (0 ppm). Complete assignments were based on two-dimensional experiments (COSY, HSQC, HMBC) using standard pulse sequences. FT-IR spectra were collected in DCM solution on a JASCO 4700 series FT-IR spectrometer in transmission mode using a liquid cell with CaF_2 windows. UV−vis spectra were recorded in toluene solution on an Agilent Technologies 8453 UV−vis spectrophotometer. Luminescence spectroscopy were measured on a Fluorolog-3 spectrometer from HORIBA Jobin Yvon.

X-ray diffraction data were collected at 100 K on a Bruker D8 Venture diffractometer with a Mo Kα (λ = 0.71073 Å) (compounds **3** and **4**) or Cu Kα (λ = 1.54178 Å) (compound **5b**) radiation source. Crystal structures were refined using the SHELXL[62] software (Table 3). Non-hydrogen atoms were refined anisotropically.

Computational Details. Density functional theory (DFT) calculations were carried out in Gaussian 16 Revision C.02[63] software and visualized using Gaussview 6[64] or Avogadro.[65] Geometry optimizations in the ground state were performed in the gas phase at a MN15L[51] level of theory combined with a triple ζ-basis set: def2tzvp.[52] The carbonyl frequency values were scaled using a factor of 0.9578[66] (see Table S1). TDDFT calculations were performed on the optimized structures at the CAM-B3LYP/def2tzvp level of theory. The solvent effect was simulated using the continuum polarized model (CPM).[67]

Procedure for the Synthesis of Complexes 1−4. Equimolar amounts of [$ReBr(CO)_5$] and the corresponding ligand were poured into a two-necked round bottom flask and dissolved in 20 mL of toluene. The reaction was heated up at reflux for 1 h observing that the mixture darkened upon completion. The solvent was evaporated to dryness. Specific details for the purification of the entitled complexes are mentioned below.

1 ($C_{22}H_{16}BrN_4O_3Re$). [$ReBr(CO)_5$] (0.0934 g, 0.230 mmol), **L1H** (0.06938 g, 0.230 mmol). Work-up: 5 mL of pentane was added to the mixture, and the crude was stirred for 30 min allowing the formation of a dark-crimson solid material. The compound was filtered out and rinsed with pentane (3 × 5 mL). (41.8 mg, 27.9%). ^{1}H NMR ($CDCl_3$, 25 °C, 400 MHz) δ/ppm: 7.30 (d, 2 H, ^3J = 8 Hz, Ph-NH *o*-H), 7.39 (t, 1 H, ^3J = 8 Hz, Ph-NH *p*-H), 7.45−7.57 (m, 5H, Ph-NH *m*-H, Ph-N=N *m*-H, Ph-NC *p*-H), 7.64 (m, 3H, Ph-NC *m*-H, Ph-N=N p-H,) 7.84 (d, 2 H, ^3J = 8 Hz, Ph-NC *o*-H), 7.89 (d, 2 H, ^3J = 8 Hz, Ph-N=N *o*-H), 8.58 (s, 1 H, NH). ^{13}C{^{1}H} NMR ($CDCl_3$, 25 °C, 150 MHz) δ/ppm: 123.21 (Ph-NH *o*-CH), 123.95 (Ph-N=N *o*-CH), 127.90 (Ph-NH *p*-CH), 128.48 (Ph-CN *ipso*-C), 128.93 (Ph-CN *o*-CH), 129.31 (Ph-N=N *m*-CH), 129.39 (Ph-NH *m*-CH), 130.10 (Ph-CN *m*-CH), 131.69 (Ph-N=N *p*-CH), 131.86 (Ph-CN *p*-CH), 140.83 (Ph-NH *ipso*-C), 157.20 (Ph-N=N *ipso*-C), 164.65 (NCN C), 185.33 (CO *trans* Br C), 192.35 (CO *trans* Ph-NH-N C), 192.89 (CO *trans* Ph-N=N C). IR(CH_2Cl_2) ν(CO)/cm^{-1}: 2035(s), 1959(s), 1923(s). MS (FAB+) (m/z): $[MH + 2]^+$ = 653, $[MH]^+$ = 651, $[MH\text{-}CO]^+$ = 623, $[MH\text{-}3CO]^+$ = 567. HRMS (ESI +) (m/z): Calcd. for $[MH]^+$ = 651.004167. Found = 651.00337. $[MH\text{-}3CO]^+$ = 567.01942. Found = 567.01817.

https://doi.org/10.1021/acs.inorgchem.2c02168
Inorg. Chem. 2022, 61, 13532−13542

2 ($C_{23}H_{18}BrN_4O_3Re$). [ReBr(CO)$_5$] (0.1235 g, 0.304 mmol), **L2H** (0.0959 g 0.305 mmol). Work-up: similar to the procedure described above. (93.3 mg, 46.0%). ^{1}H NMR ($CDCl_3$, 25 °C, 600 MHz) δ/ppm: 2.47 (s, 1 H, CH_3), 7.29 (d, 2 H, ^3J = 8 Hz, Ph-NH *o*-H), 7.38 (t, 1 H, ^3J = 7 Hz, Ph-NH *p*-H), 7.43−7.56 (m, 7H, Ph-NH *m*-H, Ph-N=N *m*-H, *p*-tol *m*-H, Ph-N=N *p*-H), 7.74 (d, 2 H, ^3J = 8 Hz, *p*-tol *o*-H), 7.88 (d, 2 H, ^3J = 7 Hz, Ph-N=N *o*-H), 8.56 (s, 1 H, NH). ^{13}C{^{1}H} NMR ($CDCl_3$, 25 °C, 150 MHz) δ/ppm: 21.71 (CH_3), 123.11 (Ph-NH *o*-CH), 123.97 (Ph-N=N *o*-CH), 125.58 (*p*-tol *ipso*-C), 127.75 (Ph-NH *p*-CH), 128.85 (*p*-tol *o*-CH), 129.29 (Ph-NH *m*-CH), 129.40 (Ph-N=N *m*-CH), 130.72 (*p*-tol *m*-CH), 131.65 (Ph-N=N *p*-CH), 140.96 (Ph-NH *ipso*-C), 142.49 (*p*-tol *p*-C), 157.24 (Ph-N=N *ipso*-C), 165.02 (NCN C), 185.37 (CO *trans* Br C), 192.40 (CO *trans* Ph-NH-N C), 192.88 (CO *trans* Ph-N=N C). IR(CH_2Cl_2) ν(CO)/cm^{-1}: 2035(s), 1959(s), 1924(s). MS (DART+) (*m*/*z*): [MH + 2]$^+$ = 667, [MH]$^+$ = 665, [MH-CO]$^+$ = 637, [MH-2CO]$^+$ = 609, [MH-3CO]$^+$ = 581. HRMS (ESI+) (*m*/*z*): Calcd. for [MH] $^+$ = 665.01982. Found = 665.01917 [MH-3CO]$^+$ = 581.035072. Found = 581.03365.

3 ($C_{23}H_{18}BrN_4O_4Re$). [ReBr(CO)$_5$] (0.0930 g, 0.229 mmol), **L3H** (0.0758 g, 0.229 mmol). Work-up: the compound was recrystallized by slow diffusion of 15 mL of pentane into 5 mL of a DCM solution of **3**. The system was kept in the freezer for 1 day allowing the formation of crystalline material. The solid was washed with 3 × 5 mL of pentane. (105 mg, 67.07%). ^{1}H NMR ($CDCl_3$, 25 °C, 600 MHz) δ/ppm: 3.88 (s, 1 H, CH_3O H), 7.10 (d, 2 H, ^3J = 8 Hz, *p*-CH_3OPh *m*-H), 7.27 (d, 2 H, ^3J = 8 Hz, Ph-NH *o*-H), 7.35 (t, 1 H, ^3J = 8 Hz, Ph-NH *p*-H), 7.45 (t, 2H, ^3J = 8 Hz, Ph-N=N *m*-H), 7.49 (t, 2H, ^3J = 8 Hz, Ph-NH *m*-H), 7.53 (t, 1H, ^3J = 7 Hz, Ph-N=N *p*-H), 7.81 (d, 2 H, ^3J = 6 Hz, *p*-CH_3OPh *o*-H), 7.88 (d, 2 H, ^3J = 8 Hz, Ph-N=N *o*-H), 8.47 (s, 1 H, NH). ^{13}C{^{1}H} NMR ($CDCl_3$, 25 °C, 150 MHz) δ/ppm: 55.64 (CH_3O, C), 115.39 (*p*-CH_3OPh *m*-CH), 120.64 (*p*-CH_3OPh *ipso*-C), 122.80 (Ph-NH *o*-CH), 123.96 (Ph-N=N *o*-CH), 127.52 (Ph-NH *p*-CH), 129.29 (Ph-NH *m*-CH), 129.41 (Ph-N=N *m*-CH), 130.82 (*p*-CH_3OPh *o*-CH), 131.68 (Ph-N=N *p*-CH), 141.14 (Ph-NH *ipso*-CH), 157.26 (Ph-N=N *ipso*-C), 162.17 (*p*-CH_3OPh *p*-C), 165.25 (NCN C), 185.38 (CO *trans* Br C), 192.40 (CO *trans* Ph-NH-N C), 192.92 (CO *trans* Ph-N=C C). IR(CH_2Cl_2) ν(CO)/cm^{-1}: 2034(s), 1958(m), 1923(s). MS (DART+) (*m*/*z*): [MH + 2]$^+$ = 683, [MH]$^+$ = 681, [MH-CO]$^+$ = 653, [MH-2CO]$^+$ = 625, [MH-3CO]$^+$ = 597. Anal. Calcd. For ($C_{23}H_{18}BrN_4O_4Re$): C 40.59, H 2.67, N 8.23; found C 39.81, H 2.59, N 7.90.

4 ($C_{22}H_{15}BrFN_4O_3Re$). [ReBr(CO)$_5$] (0.0951 g, 0.234 mmol), **L4H** (0.0745 g, 0.234 mmol). Work-up: after solvent evaporation, the crude was recrystallized by diffusion of pentane into a $CHCl_3$ solution at −30 °C. The crystalline material was filtered out and rinsed with 3 × 5 mL of pentane. (96 mg, 61.3%). ^{1}H NMR ($CDCl_3$, 25 °C, 600 MHz) δ/ppm: 7.32 (d, 2H, ^3J = 8 Hz, Ph-NH *o*-H), 7.35 (t, 2H, $^3J_{H\text{-}H}$ = 8 Hz, $^3J_{H\text{-}F}$ = 8 Hz, *p*-FPh *m*-H), 7.41 (t, 1H, ^3J = 7 Hz, Ph-NH *p*-H), 7.49 (t, 2H, , ^3J = 8 Hz, Ph-NH *m*-H), 7.54 (t, 2H, ^3J = 8 Hz, Ph-N=N *m*-H), 7.58 (t, 1H, ^3J = 7 Hz, Ph-N=N *p*-H), 7.90 (m, 4H, Ph-N=N *o*-H, *p*-FPh *o*-H), 8.42 (s, 1H, NH). ^{19}F NMR ($CDCl_3$, 25 °C, 565 MHz) δ/ppm: −105.92 (m, *p*-FPh F). ^{13}C{^{1}H} NMR ($CDCl_3$, 25 °C, 150 MHz) δ/ppm: 117.38 ($^2J_{C\text{-}F}$ = 22 Hz , *p*-FPh *m*-CH), 122.88 (Ph-NH *o*-CH), 123.94 (Ph-N=N *o*-CH), 124.74 ($^4J_{C\text{-}F}$ = 3 Hz, *p*-FPh *ipso*-C), 127.85 (Ph-NH *p*-CH), 129.36 (Ph-N=N *m*-CH), 129.47 (Ph-NH *m*-CH), 131.51 ($^3J_{C\text{-}F}$ = 9 Hz, *p*-FPh *o*-CH), 131.80 (Ph-N=N *p*-CH), 140.92 (Ph-NH *ipso*-C), 157.30 (Ph-N=N *ipso*-C), 164.39 ($J_{C\text{-}F}$ = 253.5 Hz, *p*-FPh *p*-C), 164.26 (NCN C), 185.25 (CO *trans* Br C), 192.14 (CO *trans* Ph-NH-N C), 192.63 (CO *trans* Ph-N=C C). IR(CH_2Cl_2) ν(CO)/cm^{-1}: 2036(s), 1961(s), 1925(s). MS (DART +) (*m*/*z*): [MH]$^+$ = 669, [M-CO]$^+$ = 641, [M-3CO] = 585. Anal. Calcd. For ($C_{22}H_{15}BrFN_4O_3Re$): C 39.53, H 2.26, N 8.38; found C 39.12, H 2.04, N 8.29.

5a and 5b ($C_{26}H_{24}BrN_4O_3Re$). [ReBr(CO)$_5$] (0.0886 g, 0.22 mmol) and **L5H** (0.0778 g, 0.022 mmol) were dissolved in 20 mL of toluene and heated in refluxing toluene for 2.5 h. An oily material was afforded after removal of the volatiles; then, the crude was triturated with 5 mL of pentane, yielding a dark solid. (95 mg, 61.5%). ^{1}H NMR ($CDCl_3$, 25 °C, 600 MHz) δ/ppm: (**5a**) 1.99 (s, 3H, *p*-tol *p*-CH_3), 2.05 (s, 3H, Mes-N=N *p*-CH_3), 2.07 (s, 3H, Mes-N=N *o*-CH_3), 2.81 (s, 3H, Mes-N=N *o*-CH_3), 6.64 (s, 1H, Mes-N=N *m*-H), 6.71 (s, 1H, Mes-N=N *m*-H), 6.82 (d, 2H, , ^3J = 6 Hz, Ph-NH *o*-H), 6.93 (m, 3H, Ph-NH *p*-H, *p*-tol *m*-H), 7.05 (t, 2H, ^3J = 6 Hz, Ph-NH *m*-H), 7.68 (d, 2H, ^3J = 6 Hz, *p*-tol *o*-H), 8.22 (s, 1H, NH). (**5b**) 2.05 (s, 3H, Mes-NH *p*-CH_3), 2.05 (s, 3H, Mes-NH *o*-CH_3), 2.09 (s, 3H, *p*-tol *p*-CH_3), 2.41 (s, 3H, Mes-NH *o*-CH_3), 6.70 (s, 2H, Mes-NH *m*-H), 6.93 (m, 3H, Ph-N=N *p*-H, *m*-H), 6.99 (d, 2H, ^3J = 6 Hz, *p*-tol *m*-H), 7.47 (d, 2H, ^3J = 6 Hz, *p*-tol *o*-H), 7.61 (s, 1H, NH). 7.85 (m, 2H, Ph-N=N *o*-H). ^{13}C{^{1}H} NMR ($CDCl_3$, 25 °C, 150 MHz) δ/ppm: (**5a**) 17.80 (Mes *o*-CH_3), 20.42 (Mes *o*-CH_3), 20.80 (Mes *p*-CH_3), 21.37 (*p*-tol *p*-CH_3) , 121.53 (Ph *o*-CH), 126.68(*p*-tol *p*-C), 126.94 (Ph *m*-CH), 128.6 (Mes *m*-C), 129.24 (*p*-tol *o*-CH), 129.47 17 (Mes *o*-C), 130.17 (Mes *m*-C), 130.48 (*p*-tol *m*-CH), 131.17 (Mes *o*-C), 138.18 (Mes *p*-C), 142.20 (Ph *ipso*-C), 142.20 (*p*-tol *ipso*-C) , 155.20 (Mes *ipso*-C), 167.11 (NNCN C), 186.34 (CO *trans* Br C), 192.25 (CO *trans* Mes-N=N C), 193.04 (CO *trans* PhN-NH C). (**5b**) 18.61 (Mes *p*-CH_3), 19.56 (Mes *o*-CH_3), 21.14 (Mes *o*-CH_3), 21.33 (*p*-tol *p*-CH_3), 124.09 (Ph *o*-CH), 129.14 (*p*-tol *p*-C), 129.43 (*p*-tol *o*-CH), 129.49 (Mes *m*-C), 129.93 (Mes *m*-C), 130.94 (*p*-tol *m*-CH), 131.23 (Ph *m*-CH), 136.53 (Mes *ipso*-C), 137.70 (Mes *o*-C), 137.89 (Mes *o*-C), 140.68 (Mes *p*-C), 141.79 (*p*-tol *ipso*-C), 157.15 (Ph *ipso*-C), 161.04 (NNCN C), 184.77 (CO *trans* Br C), 192.29 (CO *trans* Mes-NH C), 194.16 (CO *trans* Ph-N=N C). IR(CH_2Cl_2) ν(CO)/cm^{-1}: 2036(s), 1959(s), 1922(s). MS (DART+) (*m*/*z*): [MH + 2]$^+$ = 709, [MH]$^+$ = 707, [MH-CO]$^+$ = 678, [MH-3CO]$^+$ = 623. HRMS (ESI+) (*m*/*z*): Calcd. for [MH] $^+$ = 707.06677. Found = 707.06667. [MH-2CO]$^+$ = 651.07684. Found = 651.07610. [MH-3CO]$^+$ = 623.08193. Found = 623.08092.

■ ASSOCIATED CONTENT

Supporting Information

The Supporting Information is available free of charge at https://pubs.acs.org/doi/10.1021/acs.inorgchem.2c02168.

1D (^{1}H, ^{13}C{^{1}H}) and 2D (^{1}H EXSY) NMR experiments, additional electronic spectroscopy measurements, and computational data (geometry optimizations, TDDFT calculations, and NTO analysis) (PDF)

Accession Codes

CCDC 2180752−2180754 contain the supplementary crystallographic data for this paper. These data can be obtained free of charge via www.ccdc.cam.ac.uk/data_request/cif, or by emailing data_request@ccdc.cam.ac.uk, or by contacting The Cambridge Crystallographic Data Centre, 12 Union Road, Cambridge CB2 1EZ, UK; fax: +44 1223 336033.

■ AUTHOR INFORMATION

Corresponding Authors

Noé Zúñiga-Villarreal − *Instituto de Química, Universidad Nacional Autónoma de México, Ciudad Universitaria, 04510 México, México*; Email: zuniga@unam.mx

Edwin Otten − *Stratingh Institute for Chemistry, University of Groningen, 9747 AG, Groningen, The Netherlands*; orcid.org/0000-0002-5905-5108; Email: edwin.otten@rug.nl

Authors

Liliana Capulín Flores − *Stratingh Institute for Chemistry, University of Groningen, 9747 AG, Groningen, The Netherlands; Instituto de Química, Universidad Nacional Autónoma de México, Ciudad Universitaria, 04510 México, México*

Lucas A. Paul − *Universität Göttingen, Institut für Anorganische Chemie, D-37077 Göttingen, Germany*

Inke Siewert − *Universität Göttingen, Institut für Anorganische Chemie, D-37077 Göttingen, Germany;* orcid.org/0000-0003-3121-3917

Remco Havenith − *Stratingh Institute for Chemistry, University of Groningen, 9747 AG, Groningen, The Netherlands;* orcid.org/0000-0003-0038-6030

Complete contact information is available at: https://pubs.acs.org/10.1021/acs.inorgchem.2c02168

Author Contributions

The manuscript was written through contributions of all authors. All authors have given approval to the final version of the manuscript.

Notes

The authors declare no competing financial interest.

■ ACKNOWLEDGMENTS

Dr. F. Cortés-Guzmán and L.G. Ramírez-Palma are acknowledged for sharing computational resources as well as E. Huerta-Salazar, B. Quiroz-García, and F.J. Pérez-Flores for technical assistance (Instituto de Química, UNAM). Funding from DGAPA-UNAM (PAPIIT IN205218 and IN214220) are deeply acknowledged. Part of the computational studies was carried out on the Dutch national e-infrastructure (Snellius@ Surfsara). L.C.F. acknowledges a Ph.D. stipend from CONACyT and the University of Groningen.

■ REFERENCES

(1) Maslakova, T. I.; Lipunov, I. N.; Pervova, I. G.; Maslakov, P. A. Formazan-Containing Solid-Phase Reagent Indicator Systems for Environmental Analysis. *Russ. J. Gen. Chem.* **2018**, *88*, 2717−2731.

(2) Ciapetti, G.; Cenni, E.; Pratelli, L.; Pizzoferrato, A. In Vitro Evaluation of Cell/Biomaterial Interaction by MTT Assay. *Biomaterials* **1993**, *14*, 359−364.

(3) Szymczyk, M.; El-shafei, A.; Freeman, H. S. Design , Synthesis , and Characterization of New Iron-Complexed Azo Dyes. *Dyes Pigm.* **2007**, *72*, 8−15.

(4) Gilroy, J. B.; McKinnon, S. D. J.; Koivisto, B. D.; Hicks, R. G. Electrochemical Studies of Verdazyl Radicals. *Org. Lett.* **2007**, *9*, 4837−4840.

(5) Hunter, L.; Roberts, C. B. The Azo-Group as a Chelating Group. Part V. Metallic Derivatives of Arylazo-Oximes and of Formazyl Compounds. *J. Chem. Soc.* **1941**, 823−826.

(6) Barbon, S. M.; Price, J. T.; Reinkeluers, P. A.; Gilroy, J. B. Substituent-Dependent Optical and Electrochemical Properties of Triarylformazanate Boron Difluoride Complexes. *Inorg. Chem.* **2014**, *53*, 10585−10593.

(7) Gilroy, J. B.; Otten, E. Formazanate Coordination Compounds: Synthesis, Reactivity, and Applications. *Chem. Soc. Rev.* **2020**, *49*, 85−113.

(8) de Vries, F.; Otten, E. Reversible On/Off Switching of Lactide Cyclopolymerization with a Redox-Active Formazanate Ligand. *ACS Catal.* **2022**, *12*, 4125−4130.

(9) Chang, M. C.; Roewen, P.; Travieso-Puente, R.; Lutz, M.; Otten, E. Formazanate Ligands as Structurally Versatile, Redox-Active Analogues of *β*-Diketiminates in Zinc Chemistry. *Inorg. Chem.* **2015**, *54*, 379−388.

(10) Zhao, B.; Han, Z.; Ding, K. The N-H Functional Group in Organometallic Catalysis. *Angew. Chem., Int. Ed.* **2013**, *52*, 4744−4788.

(11) Wu, H. L.; Li, X. B.; Tung, C. H.; Wu, L. Z. Bioinspired Metal Complexes for Energy-Related Photocatalytic Small Molecule Transformation. *Chem. Commun.* **2020**, *56*, 15496−15512.

(12) Drosou, M.; Kamatsos, F.; Mitsopoulou, C. A. Recent Advances in the Mechanisms of the Hydrogen Evolution Reaction by Non-Innocent Sulfur-Coordinating Metal Complexes. *Inorg. Chem. Front.* **2020**, *7*, 37−71.

(13) Siewert, I. Electrochemical CO_2 Reduction Catalyzed by Binuclear $LRe_2(CO)_6Cl_2$ and $LMn_2(CO)_6Br_2$ Complexes with an Internal Proton Source. *Acc. Chem. Res.* **2022**, *55*, 473−483.

(14) Fujita, E.; Grills, D. C.; Manbeck, G. F.; Polyansky, D. E. Understanding the Role of Inter- and Intramolecular Promoters in Electro- and Photochemical CO_2 Reduction Using Mn, Re, and Ru Catalysts. *Acc. Chem. Res.* **2022**, *55*, 616−628.

(15) Drover, M. W. A Guide to Secondary Coordination Sphere Editing. *Chem. Soc. Rev.* **2022**, *51*, 1861−1880.

(16) Gallardo-Villagrán, M.; Rivada-Wheelaghan, O.; Rahaman, S. M. W.; Fayzullin, R. R.; Khusnutdinova, J. R. Proton-Responsive Naphthyridinone-Based Ru(II) Complexes and Their Reactivity with Water and Alcohols. *Dalton Trans.* **2020**, *49*, 12756−12766.

(17) Zhou, C.; Hu, J.; Wang, Y.; Yao, C.; Chakraborty, P.; Li, H.; Guan, C.; Huang, M. H.; Huang, K. W. Selective Carbonylation of Benzene to Benzaldehyde Using a Phosphorus-Nitrogen PN^3P-Rhodium(I) Complex. *Org. Chem. Front.* **2019**, *6*, 721−724.

(18) Mukherjee, J.; Siewert, I. Manganese and Rhenium Tricarbonyl Complexes Equipped with Proton Relays in the Electrochemical CO_2 Reduction Reaction. *Eur. J. Inorg. Chem.* **2020**, *2020*, 4319−4333.

(19) Darshani, T.; Thushara, N.; Weerasuriya, P.; Fronczek, F. R.; Perera, I. C.; Perera, T. Fluorescent Di-(2-Picolyl)Amine Based Drug-like Ligands and Their $Re(CO)_3$ Complexes towards Biological Applications. *Polyhedron* **2020**, *185*, No. 114592.

(20) Gaire, S.; Schrage, B. R.; Ziegler, C. J. An Organometallic Isostere of an Amino Acid. *Inorg. Chem.* **2021**, *60*, 10105−10108.

(21) Auvray, T.; Pal, A. K.; Hanan, G. S. Electronic Properties of Rhenium(I) Carbonyl Complexes Bearing Strongly Donating Hexahydro-Pyrimidopyrimidine Based Ligands. *Eur. J. Inorg. Chem.* **2021**, *2021*, 2570−2577.

(22) Gonçalves, M. R.; Benvenho, A. R. V.; Frin, K. P. M. Electrical and Optical Properties of Organic Light-Emitting Diodes with Rhenium(I) Complexes Using DC and AC Methods. *Opt. Mater.* **2019**, *94*, 206−212.

(23) Deeba, R.; Molton, F.; Chardon-Noblat, S.; Costentin, C. Effective Homogeneous Catalysis of Electrochemical Reduction of Nitrous Oxide to Dinitrogen at Rhenium Carbonyl Catalysts. *ACS Catal.* **2021**, *11*, 6099−6103.

(24) Hellman, A. N.; Haiges, R.; Marinescu, S. C. Rhenium Bipyridine Catalysts with Hydrogen Bonding Pendant Amines for CO_2 Reduction. *Dalton Trans.* **2019**, *48*, 14251−14255.

(25) Riplinger, C.; Carter, E. A. Influence of Weak Bronsted Acids on Electrocatalytic CO_2 Reduction by Manganese and Rhenium Bipyridine Catalysts. *ACS Catal.* **2015**, *5*, 900−908.

(26) Wong, K. Y.; Chung, W. H.; Lau, C. P. The Effect of Weak Brönsted Acids on the Electrocatalytic Reduction of Carbon Dioxide by a Rhenium Tricarbonyl Bipyridyl Complex. *J. Electroanal. Chem.* **1998**, *453*, 161−170.

(27) Sinha, S.; Berdichevsky, E. K.; Warren, J. J. Electrocatalytic CO_2 Reduction Using Rhenium(I) Complexes with Modified 2-(2'-Pyridyl)Imidazole Ligands. *Inorg. Chim. Acta* **2017**, *460*, 63−68.

(28) Sung, S.; Kumar, D.; Gil-Sepulcre, M.; Nippe, M. Electrocatalytic CO_2 Reduction by Imidazolium-Functionalized Molecular Catalysts. *J. Am. Chem. Soc.* **2017**, *139*, 13993−13996.

(29) Manbeck, G. F.; Muckerman, J. T.; Szalda, D. J.; Himeda, Y.; Fujita, E. Push or Pull? Proton Responsive Ligand Effects in Rhenium Tricarbonyl CO_2 Reduction Catalysts. *J. Phys. Chem. B* **2015**, *119*, 7457−7466.

(30) Rotundo, L.; Polyansky, D. E.; Gobetto, R.; Grills, D. C.; Fujita, E.; Nervi, C.; Manbeck, G. F. Molecular Catalysts with Intramolecular Re − O Bond for Electrochemical Reduction of Carbon Dioxide. *Inorg. Chem.* **2020**, *59*, 12187−12199.

(31) Jia-Pei, D.; Wilting, A.; Siewert, I. Are Two Metal Ions Better than One? Mono and Binuclear Alfa-Diimine-$Re(CO)_3$ Complexes with Proton-Responsive Ligands in CO_2 Reduction Catalysis. *Chem. − Eur. J.* **2019**, *25*, 5555−5564.

(32) Vollmer, M. V.; Machan, C. W.; Clark, M. L.; Antholine, W. E.; Agarwal, J.; Schaefer, H. F.; Kubiak, C. P.; Walensky, J. R. Synthesis, Spectroscopy, and Electrochemistry of (α-Diimine)M(CO)$_3$Br, M = Mn, Re, Complexes: Ligands Isoelectronic to Bipyridyl Show Differences in CO_2 Reduction. *Organometallics* **2015**, *34*, 3−12.
(33) Mckinnon, M.; Ngo, K. T.; Sobottka, S.; Sarkar, B.; Ertem, M. Z.; Grills, D. C.; Rochford, J. Synergistic Metal−Ligand Redox Cooperativity for Electrocatalytic CO_2 Reduction Promoted by a Ligand-Based Redox Couple in Mn and Re Tricarbonyl Complexes. *Organometallics* **2019**, *38*, 1317−1329.
(34) Benson, E. E.; Sampson, M. D.; Grice, K. A.; Smieja, J. M.; Froehlich, J. D.; Friebel, D.; Keith, J. A.; Carter, E. A.; Nilsson, A.; Kubiak, C. P. The Electronic States of Rhenium Bipyridyl Electrocatalysts for CO_2 Reduction as Revealed by X-Ray Absorption Spectroscopy and Computational Quantum Chemistry. *Angew. Chem., Int. Ed.* **2013**, *52*, 4841−4844.
(35) Matson, B. D.; McLoughlin, E. A.; Armstrong, K. C.; Waymouth, R. M.; Sarangi, R. Effect of Redox Active Ligands on the Electrochemical Properties of Manganese Tricarbonyl Complexes. *Inorg. Chem.* **2019**, *58*, 7453−7465.
(36) Queyriaux, N. Redox-Active Ligands in Electroassisted Catalytic H^+ and CO_2 Reductions: Benefits and Risks. *ACS Catal.* **2021**, 4024−4035.
(37) Travieso-Puente, R.; Chang, M. C.; Otten, E. Alkali Metal Salts of Formazanate Ligands: Diverse Coordination Modes as a Result of the Nitrogen-Rich [NNCNN] Ligand Backbone. *Dalton Trans.* **2014**, *43*, 18035−18041.
(38) Baumgardner, D. F.; Parks, W. E.; Gilbertson, J. D. Harnessing the Active Site Triad: Merging Hemilability, Proton Responsivity, and Ligand-Based Redox-Activity. *Dalton Trans.* **2020**, *49*, 960−965.
(39) Tiers, G.; Plovan, S.; Searles, S. Proton Nuclear Resonance Spectroscopy. Rapid Tautomerization of Formazans. *J. Org. Chem.* **1960**, *25*, 285−286.
(40) Sigeikin, G. I.; Lipunova, G. N.; Pervova, I. G. Formazans and Their Metal Complexes. *Russ. Chem. Rev.* **2006**, *75*, 885−900.
(41) Allen, F. H.; Watson, D. G.; Bramer, L.; Orpen, A. G.; Taylor, R. International Tables for Crystallography (2006). In *International Tables fo Crystallography*; 2006; Vol. *C*, pp. 790−811.
(42) Chakraborty, I.; Carrington, S. J.; Mascharak, P. K. Photodelivery of CO by Designed PhotoCORMs: Correlation between Absorption in the Visible Region and Metal-CO Bond Labilization in Carbonyl Complexes. *ChemMedChem* **2014**, *9*, 1266−1274.
(43) Kottelat, E.; Lucarini, F.; Crochet, A.; Ruggi, A.; Zobi, F. Correlation of MLCTs of Group 7 *fac*-[M(CO)$_3$]$^+$ Complexes (M = Mn, Re) with Bipyridine, Pyridinylpyrazine, Azopyridine, and Pyridin-2-Ylmethanimine Type Ligands for Rational PhotoCORM Design. *Eur. J. Inorg. Chem.* **2019**, 3758−3768.
(44) Samanta, S.; Ghosh, P.; Goswami, S. Recent Advances on the Chemistry of Transition Metal Complexes of 2-(Arylazo)Pyridines and Its Derivatives. *Dalton Trans.* **2012**, *41*, 2213−2226.
(45) Roy, S.; Sieger, M.; Sarkar, B.; Schwerdeski, B.; Lissner, F.; Schleid, T.; Fiedler, J.; Kaim, W. Establishing the Chelating Alfa-Azocarbonyl Function in Pi-Acceptor Ligands. *Angew. Chem., Int. Ed.* **2008**, *47*, 6192−6194.
(46) Carrington, S. J.; Chakraborty, I.; Alvarado, J. R.; Mascharak, P. K. Differences in the CO Photolability of *Cis*- and *Trans*-[RuCl$_2$(Azpy)(CO)$_2$] Complexes: Effect of Metal-to-Ligand Back-Bonding. *Inorg. Chim. Acta* **2013**, *407*, 121−125.
(47) Wei, L.; Babich, J. W.; Ouellette, W.; Zubieta, J. Developing the {M(CO)$_3$}$^+$ Core for Fluorescence Applications: Rhenium Tricarbonyl Core Complexes with Benzimidazole, Quinoline, and Tryptophan Derivatives. *Inorg. Chem.* **2006**, *45*, 3057−3066.
(48) Morimoto, T.; Ito, M.; Koike, K.; Kojima, T.; Ozeki, T.; Ishitani, O. Dual Emission from Rhenium(I) Complexes Induced by an Interligand Aromatic Interaction. *Chem. − Eur. J.* **2012**, *18*, 3292−3304.
(49) Milocco, F.; De Vries, F.; Bartels, I. M. A.; Havenith, R. W. A.; Cirera, J.; Demeshko, S.; Meyer, F.; Otten, E. Electronic Control of Spin-Crossover Properties in Four-Coordinate Bis(Formazanate) Iron(II) Complexes. *J. Am. Chem. Soc.* **2020**, *142*, 20170−20181.
(50) Chang, M. C.; Otten, E. Synthesis and Ligand-Based Reduction Chemistry of Boron Difluoride Complexes with Redox-Active Formazanate Ligands. *Chem. Commun.* **2014**, *50*, 7431−7433.
(51) Yu, H. S.; He, X.; Truhlar, D. G. MN15-L: A New Local Exchange-Correlation Functional for Kohn-Sham Density Functional Theory with Broad Accuracy for Atoms, Molecules, and Solids. *J. Chem. Theory Comput.* **2016**, *12*, 1280−1293.
(52) Weigend, F.; Ahlrichs, R. Balanced Basis Sets of Split Valence, Triple Zeta Valence and Quadruple Zeta Valence Quality for H to Rn: Design and Assessment of Accuracy. *Phys. Chem. Chem. Phys.* **2005**, *7*, 3297−3305.
(53) Leirer, M.; Knör, G.; Vogler, A. Synthesis and Spectroscopic Properties of 1,2-Diiminetricarbonylrhenium(I)Chloride Complexes with Aliphatic Diimines (or 1,4-Diaza-1,3-Butadienes) as Ligands. *Zeitschrift fur Naturforschung B* **1999**, *54*, 341−344.
(54) Klemens, T.; Świtlicka, A.; Szlapa-Kula, A.; Łapok, Ł.; Obłoza, M.; Siwy, M.; Szalkowski, M.; MaćKowski, S.; Libera, M.; Schab-Balcerzak, E.; MacHura, B. Tuning Optical Properties of Re(I) Carbonyl Complexes by Modifying Push-Pull Ligands Structure. *Organometallics* **2019**, *38*, 4206−4223.
(55) Stout, M. J.; Skelton, B. W.; Sobolev, A. N.; Raiteri, P.; Massi, M.; Simpson, P. V. Synthesis and Photochemical Properties of Re(I) Tricarbonyl Complexes Bound to Thione and Thiazol-2-Ylidene Ligands. *Organometallics* **2020**, *39*, 3202−3211.
(56) Kumar, A.; Sun, S.-S.; Lees, A. J. Photophysics and Photochemistry of Organometallic Rhenium Diimine Complexes. In *Photophysics of Organometallics*; Lees, A. J., Ed.; Springer Berlin, Heidelberg: Binghamton, NY, 2010; p 240.
(57) Worl, L. A.; Duesing, R.; Chen, P.; Ciana, L. Della; Meyer, T. J. Photophysical Properties of Polypyridyl Carbonyl Complexes of Rhenium(I). *J. Chem. Soc., Dalton Trans.* **1991**, 849−858.
(58) Chang, M. C.; Chantzis, A.; Jacquemin, D.; Otten, E. Boron Difluorides with Formazanate Ligands: Redox-Switchable Fluorescent Dyes with Large Stokes Shifts. *Dalton Trans.* **2016**, *45*, 9477−9484.
(59) Maar, R. R.; Zhang, R.; Stephens, D. G.; Ding, Z.; Gilroy, J. B. Near-Infrared Photoluminescence and Electrochemicaluminescence from a Remarkably Simple Boro Difluoride Formazanate Dye. *Angew. Chem., Int. Ed.* **2019**, *58*, 1052−1056.
(60) Maar, R. R.; Barbon, S. M.; Sharma, N.; Groom, H.; Luyt, L. G.; Gilroy, J. B. Evaluation of Anisole-Substituted Born Difluoride Formazanate Complexes for Fluorescence Cell Imaging. *Chem. − Eur. J.* **2015**, *21*, 15589−15599.
(61) S. P., Schmidt, W. C., Trogler, F. B. Pentacarbonylrhenium, Halides. In *Inorganic syntheses*; Angelici, R. J., Ed.; Wiley, 1991; Vol. *28*, 160−165.
(62) Sheldrick, G. M. Crystal Structure Refinement with SHELXL. *Acta Crystallogr., Sect. C: Struct. Chem.* **2015**, *71*, 3−8.
(63) Frish, M. J.; Trucks, G. W.; Schlegel, H. B.; Scuseria, G. E.; Robb, M. A.; Cheeseman, J. R.; Scalmani, G.; Barone, V.; Petersson, G. A.; Nakatsuji, H. *Gaussian 16, Revision C.02*. Wallingford CT 2019.
(64) Dennington, R.; Keith, T. A.; Millam, J. M. GaussView, Version 6. Semichem Inc., Shawnee Mission: KS 2016.
(65) Hanwell, M. D.; Curtis, D. E.; Lonie, D. C.; Vandermeersch, T.; Zurek, E.; Hutchinson, G. R. Avogadro: An Advanced Semantic Chemical Editor, Visualization, and Analysis Platform. *Aust. J. Chem.* **2012**, *4*, 1−17.
(66) Sae-Heng, P.; Tantirungrotechai, J.; Tantirungrotechai, Y. Scale Factors for Carbonyl Vibrational Frequencies: A Study of Partial Hessian Approximation. *Chiang Mai J. Sci.* **2018**, *45*, 2797−2808.
(67) Miertuš, S.; Scrocco, E.; Tomasi, J. Electrostatic Interaction of a Solute with a Continuum. A Direct Utilization of AB Initio Molecular Potentials for the Prevision of Solvent Effects. *Chem. Phys.* **1981**, *55*, 117−129.

https://doi.org/10.1021/acs.inorgchem.2c02168
Inorg. Chem. 2022, 61, 13532−13542